ISIJ International, Vol. 55 (2015), No. 12, pp. 2556–2565

Factors Controlling High-temperature Zone Resistance to Airflow during Iron Ore Sintering

Hao ZHOU,* Mingxi ZHOU, Zihao LIU, Ming CHENG, Kunzan QIU and Kefa CEN

State Key Laboratory of Clean Energy Utilization, Institute for Thermal Power Engineering, Zhejiang University, Zheda road, Hangzhou, 310027 P. R. China.

(*Received on May 31, 2015; accepted on September 4, 2015*)

A fundamental study was carried out on the high-temperature zone flow resistance during iron ore sintering. In present work, firstly, quartz sand was used to replace iron ores to investigate the impact of temperature if bed structure has no change; then a three-layer bed structure was used to explore the primary factors controlling high-temperature zone structure for airflow. The zone where temperature above 700°C is defined as high temperature zone. High-temperature zone flow resistance depends on sinter bed temperature and high-temperature zone structure which was related to melt volume, melt properties, bed voidage, drive force and high temperature zone thickness. A new model $\left(k_5 = \frac{V_{pre} - V_{post}}{(V_{post})^3} * f(\beta, \mu, \gamma, \xi_0, h)\right)$ which can suggest high-temperature zone flow resistance was established by using Support Vector Machine (SVM) model and predicted airflow rate well. Drive force has a very impact on high-temperature zone flow resistance. It can dilute gas channels in the high-temperature zone and increase or maintain sinter bed permeability. Sintering under lower suction has greater high-temperature zone resistance. Too much melt will deteriorate high-temperature zone permeability; sintering airflow rate with high coke rate in the bottom layer decreases by around 25% at a suction of 8 kPa. Similarly melt properties also have a great impact on high-temperature zone resistance; high viscosity is bad for gas channels formation in the high-temperature zone. Under a limited range increasing coke rate has little influence on high-temperature zone resistance.

KEY WORDS: high-temperature zone flow resistance; iron ore; sintering.

1. Introduction

Iron ore sintering is a very important process in steel plants, which can provide iron-bearing material for blast furnace. With world steel production continually increasing, especially in Asian-Pacific region, the demand for sinter in blast furnace continues to increase. In order to meet the demand and keep economic benefit, sinter productivity must be maintained to a certain level. Sinter productivity is closely relative to sinter bed flow resistance. During iron ore sintering high-temperature zone is established after ignition, where coke particles combust and melt forms and solidifies and which is a solid-liquid-gas system with high temperature (as high as 1 350°C).[1–4] In the high-temperature zone, melt can be formed and bond iron ore and flux particles together to form the sinter which is agglomerate composed of unreacted remnant ore and solidified melt. Due to high-temperature and much melt, for general sinter bed height high-temperature zone exerts the most important influence on overall bed flow resistance although the wet zone has some effects on the bed pressure drop.[3]

After ignition, sinter bed temperatures in high-temperature zone increase and high-temperature zone structure changes because of melt formation and coalescence. These result in the change of high-temperature zone flow resistance.[3,5] According to Ergun equation,[6] bed flow resistance for air is determined by temperature and bed structure. It is very important for us to find the impact of high-temperature zone temperature and structure on high-temperature zone flow resistance during iron ore sintering. Although there are some researchers focusing on the research of high-temperature zone flow resistance,[1–5,7–9] the action of temperature and bed structure on high-temperature zone flow resistance is not very clear. Due to high temperature and melt in the high-temperature zone, it is not easy to measure high-temperature zone flow resistance. Loo[3,4] took the reduction of air flow rate after ignition to assess high-temperature zone flow resistance and proposed a semi-empirical equation to characterize the 'sinterability' of iron ore mixes. Loo[4] studied the influence of some parameters on high-temperature zone flow resistance, and found increasing basicity can lower high-temperature zone flow resistance because of lower temperature or better melt fluidity in the high-temperature zone, and pointed out that increasing the melt formation by introducing pisolite ore into sinter blend didn't alter sinter permeability. But Oyama *et al.*[7] and Kasai *et al.*[8] found that excess melt in high-temperature zone would have a detrimental effect on bed permeability.

Bed structure in high-temperature zone is very important

* Corresponding author: E-mail: zhouhao@zju.edu.cn
DOI: http://dx.doi.org/10.2355/isijinternational.ISIJINT-2015-311

for high-temperature zone resistance. If there are many large channels for airflow, this can lower high-temperature zone flow resistance. At present, there are many researchers to investigate sinter microstructure,[1,5–8] but there are few papers to report the bed structure for airflow. Loo[3] studied the relationship between green bed permeability and sintering airflow rate, found that sintering airflow rate was greater with better green bed permeability and proposed that green bed permeability may affect gas channels in the high-temperature zone. Damien[9] also found that when coarser coke was used, sinter productivity and sintering airflow rate were higher because of better green bed permeability. While, so far details that factors control high-temperature zone structure and the influence of high-temperature zone structure on high-temperature zone resistance are not very clear.

In this work, novel experiments were conducted to investigate the influence of temperature and high-temperature zone structure on high-temperature zone flow resistance. Firstly, iron ores are replaced by quartz sand and no melt could be formed, so the influence of temperature on high-temperature zone flow resistance if bed structure has no change can be investigated. During iron ore sintering, high-temperature zone flow resistance controls the overall bed flow resistance and high-temperature zone temperature and the width of the temperature profile both increase with flame front descending down.[2–4] This means that resistance of the high-temperature zone to airflow should increases with time. However, experiments involving a very wide range of test conditions have shown that the airflow rate remains relatively constant until close to burn-through.[3] This shows that high-temperature zone structure has changed to maintain sinter bed permeability. In the high-temperature zone the main change of bed structure comes from the above 1 100°C zone where melt can be formed. In this work, a sandwich bed structure was used to study the factors controlling high-temperature zone structure. A disturbance in front of the high-temperature zone is added, which is carried out by altering sinter parameters, then use the change of airflow rate to assess the change of high-temperature zone flow resistance and bed structure.

2. Experimental

2.1. Description of Sinter Pot Test

Sintering experiments were carried out to study the influence of important parameters on high-temperature zone resistance in the sinter pot which had described in Ref. 4). The raw mixture was mixed and granulated for 1 min and 10 min, respectively. After granulation, the granulated mix was loaded into the sinter pot which had an internal diameter of 335 mm and height of 600 mm. Natural gas was supplied for 90 s to ignite coke under a suction of 6 kPa, subsequently suction was raised to 16 kPa to sinter. Windbox temperature was recorded continuously by K type thermocouple and sinter fan was shut down when windbox temperature dropped below 200°C. During iron ore sintering, inlet airflow rate was recorded by TSI hot wire anemometer and transported to Agilent data acquisition instrument. Because the voltage signal of airflow rate recorded by Agilent data acquisition instrument has some noises, noises have been removed during signal processing stage and airflow rate curves were smoothed by software.

2.2. Experimental Method

In order to distinct the effect of temperature and high temperature zone structure on high temperature zone flow resistence, two kinds of blend were used. First, the raw mixture consisted of quart sand and coke was used to investigate the influence of temperature on high-temperature zone flow resistance. Because quartz sand melting point is as high as 1 600°C, there is no melt formation during sintering. We can study the impact of temperature on high-temperature zone flow resistance when bed structure has no change, then the effect of high-temperature zone structure on high-temperature zone flow resistance during iron ore sintering is clear.

When the influence of bed strucuture on high-temperature zone flow resistance was studied, the raw mixture was consisted of five kinds of iron ore(AUS1 16.7 wt.%, AUS2 16.7 wt.%, AUS3 33.3 wt.%, BRA1 16.7 wt.%, BRA2 16.7 wt.%), fluxes and coke. The chemical composition of the raw materials is given in **Table 1**.[10] Base blend details are 6.5 wt.% moisture, 1.9 basicity(CaO/SiO_2), 5.0 wt.% SiO_2, 1.7 wt.% MgO, 4.05 wt.% coke rate and 20 wt.% return fines.

In addition, for investigating the factors controlling high-temperature zone structure, a sandwich sinter bed structure was carried out in this work, as shown in **Fig. 1**. At first changes of bed properties in the middle layer were made on the basis of base blend in Fig. 1(a), and then raw materials were swapped around, the top and bottom layers in Fig.

Table 1. The chemical composition of raw materials/wt.%.[10]

Item	Fe	Al_2O_3	SiO_2	MgO	CaO	P	S	LOI1000
AUS1	60.62	2.25	4.45	0.08	0.05	0.07	0.03	5.91
ASU2	62.39	2.23	4.28	0.13	0.15	0.08	0.02	3.51
AUS3	58.07	1.26	5.09	0.07	0.08	0.04	0.02	10.20
BRA1	64.98	1.26	2.36	0.07	0.06	0.02	0.01	2.03
BRA2	64.31	0.79	5.42	0.17	0.09	0.03	0.01	1.09
Coke	1.07	4.32	6.11	0.04	0.62	0.03	0.01	86.85
Limestone	2.91	0.79	2.16	0.36	51.32	0.01	0.07	40.80
Serpentine	5.55	1.37	37.70	36.50	1.49	0.01	0.04	14.10
Dolomite	0.35	0.58	2.26	19.45	31.45	0.01	0.03	45.5

1(a) becomes the middle layer in Fig. 1(b) and middle layer in Fig. 1(a) becomes the top and bottom layers. The aim of these tests was to form a stable high-temperature zone first, and then subject it to changes of bed properties, which leaded to some changes of high-temperature zone structure and flow resistance. The changes of high-temperature zone resistance and structure are assessed and quantified in terms of changes in airflow rates through the bed as the flame front traverses the specially prepared layer. The influence of sinter parameters, such as coke rate, basicity, *etc*., on high-temperature zone resistance is also investigated by the sandwich structure, details of three-layer sinter bed conditions are showed in **Table 2**.

In this work sinter airflow rate was used to assess the change of high-temperature zone flow resistance. In order to get accurate airflow rate, an annular layer of fine sand was filled between sinter pot and the green mix.[4)]

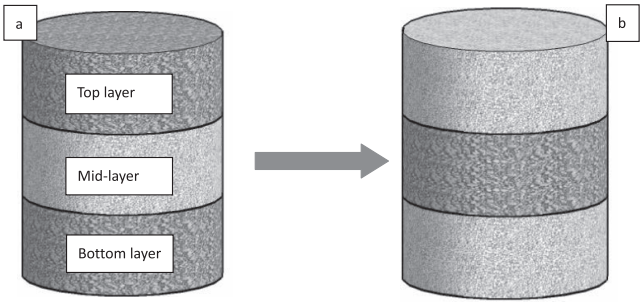

Fig. 1. Sandwich structure of the sinter bed.

Table 2. Sinter pot test conditions of three-layer bed.

Parameters	Three layers structure	Suction/kpa
Coke rate	4.05 wt.%−4.55 wt.%−4.05 wt.%	16
	4.85 wt.%−4.05 wt.%−4.85 wt.%	16
	4.05 wt.%−4.85 wt.%−4.05 wt.%	16
	4.85 wt.%−4.05 wt.%−4.85 wt.%	8
	4.05 wt.%−4.85 wt.%−4.05 wt.%	8
Basicity	2.4−1.9−2.4	16
	1.9−2.4−1.9	16
	1.9−1.4−1.9	16
	1.4−1.9−1.4	16
Coke size	Plus 1 mm-Normal-Plus 1 mm	16
	Normal-Plus 1 mm-Normal	16
	Plus 0.5 mm-Normal-Plus 0.5 mm	16
	Normal-Plus 0.5 mm-Normal	16

2.3. Method to Determine Interface between Two Layers

The typical results of three-layer sinter bed in **Fig. 2** show pre-ignition airflow rate (V_{pre}), post-ignition airflow rate (V_s) and the change of airflow rate after flame front arriving at the mid-layer. In this work airflow rate in the period from 0.1 XY to 0.9 XY, *i.e.* omitting the first and last 10% of the results, was used to assess the high-temperature zone flow resistance according to Loo's work.[3)]

In order to calculate the average post-ignition airflow rate of each layer the time which flame front gets to the interface between two layers position must be determined. And the position could be determined by two methods, shown in **Fig. 3**. Thermocouples could be located into sinter bed and record the sinter bed temperature. According to temperature curves the cross over position of flame front could be deter-

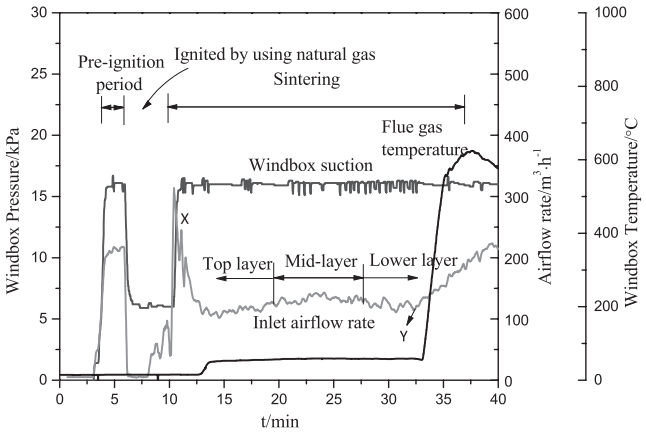

Fig. 2. Typical curves of three-layer sinter bed. X: the time where ignition just complished. Y: the time where flame front moved to the hearth layer.

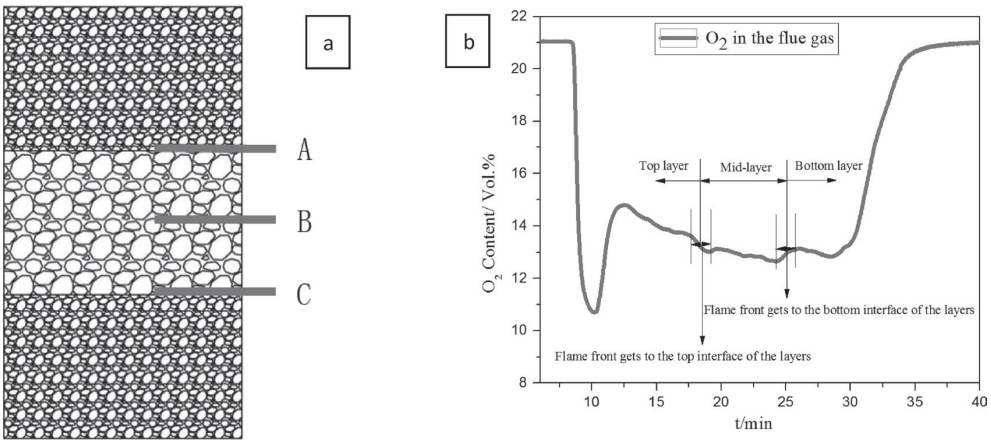

Fig. 3. Methods to determine the cross over position[10)]. A: Thermocouple located at 200 mm down stream of the bed surface. B: Thermocouple located at 300 mm down stream of the bed surface. C: Thermocouple located at 400 mm down stream of the bed surface.

mined. Bed shrinkage can affect accuracy of the cross over position. But the error coming from bed shrinkage is around 1% according to our tests, it can be acceptable. Another in this work a three-layer bed structure was adopted; waste gas composition would have a step change during flame front crossing the interface of two layers when some special parameters were changed, such as coke rate. So the time when flame front reached the middle layer or bottom layer could be obtained by measuring waste gas composition, such as CO, O_2 and NO_x. Figure 3(b) shows that we can obtain the time according to the change of O_2 content in the flue gas. And in this work when coke rate was increased to 4.55 wt.%, gas composition was not determined and thermocouple was not placed, but because airflow rate was very stable, airflow rate for each layer was calculated according to mean flame front speed.

3. Factors Influencing High-temperature Zone Flow Resistance

Momentum equation can describe the relationship between airflow rate and pressure drop through the sintering bed accurately. For the sintering bed, a special type of packed bed, Ergun equation,[6] shown in Eq. (1), can be used to calculate the sintering bed pressure drop instead of momentum equation, which has been validated by Zou *et al*.[11–15] Equation (1) shows that flow resistance in high-temperature zone is related to fluid characteristics, bed structure, and airflow rate and high-temperature zone thickness. Generally air is the fluid during iron ore sintering, so fluid characteristics are determined by bed temperature. Airflow rate and high-temperature zone thickness are both related to bed temperature closely. When bed temperature is high, airflow expands through the bed and airflow rate increases, and high-temperature zone thickness also increases. Bed structure can determine gas channels, surface flatness and tortuosity of gas channels, which can influence flow resistance strongly. In total, we can find that high-temperature zone flow resistance is mainly determined by temperature and bed structure.

$$\Delta P_{pre} = \left(150\frac{(1-\varepsilon)^2\mu}{\varepsilon^3 d^2}u + 1.75\frac{(1-\varepsilon)\rho}{\varepsilon^3 d}u^2 \right) H \quad \text{..... (1)}$$

Where, ε is bed voidage, d is particle effective diameter, μ is dynamic viscosity, u is superficial velocity, ρ is gas density, H is bed height.

3.1. Impact of Temperature on High-temperature Zone Flow Resistance

As discussed above, temperature and high-temperature zone structure both affect high-temperature zone flow resistance. During iron ore sintering, coke particles combust and sinter bed temperature increases sharply, which results in the increase of high-temperature zone flow resistance. High temperature can also result in melt formation, which has a great effect on high-temperature zone structure. The change of high-temperature zone structure can affect the high-temperature zone flow resistance in turn. During iron ore sintering, high temperature and melt formation are closely tied. It is not easy to make a distinction between the influences of temperature and high-temperature zone structure on high-temperature zone flow resistance by conventional method. So theoretical calculation and novel experiments by using quartz sand were used to investigate the influence of temperature on high-temperature zone flow resistance.

After ignition, sinter zone, high-temperature zone and wet zone are formed. High-temperature zone flow resistance controlled the sinter bed flow resistance and resistance from other regions is relatively small. Temperature in most parts of wet zone and sinter zone is near to ambient temperature. So after high-temperature zone is established, sinter bed pressure drop can be expressed by a simplified description if bed structure has no change, as shown in Eq. (2).

$$\Delta P_{post} = \Delta P_1 + \Delta P_2 = \left(150\frac{(1-\varepsilon)^2\mu_1}{\varepsilon^3 d^2}u_1 + 1.75\frac{(1-\varepsilon)\rho_1}{\varepsilon^3 d}{u_1}^2 \right) l_1 + \left(150\frac{(1-\varepsilon)^2\mu_2}{\varepsilon^3 d^2}u_2 + 1.75\frac{(1-\varepsilon)\rho_2}{\varepsilon^3 d}{u_2}^2 \right) l_2 \quad \text{..... (2)}$$

Where, ΔP_1 represents the pressure drop of normal temperature zone, ΔP_2 is the pressure drop of high temperature zone. μ_1 is airflow dynamic viscosity in normal temperature zone, μ_2 is airflow dynamic viscosity in high temperature zone, u_1 is superficial velocity in normal temperature zone, u_2 is superficial velocity in high temperature zone, ρ_1 is gas density in normal temperature zone, ρ_2 is gas density in high temperature zone, l_1 is the thickness of normal temperature zone, l_2 is the thickness of high temperature zone.

Coke particles start to combust in the zone where temperature is above 700°C.[16,17] Limestone and dolomite generally start to decompose at around 700°C. Most of the physical and chemical interactions during iron ore sintering occur above 700°C. So the zone (above 700°C) is set as high temperature zone. During iron ore sintering absolute pressure in the normal temperature zone is similar to that in high temperature zone. So if high-temperature zone structure has no change, the relationship between gas flow velocities in high and normal temperature zones can be expressed approximately by Eq. (3).

$$u_2 = \alpha u_1 = \frac{T_2}{T_1}u_1 \quad \text{..... (3)}$$

Where, T_2 is the temperature in high temperature zone (above 700°C), T_1 is the temperature in normal temperature zone (below 700°C). The relationship between post and pre-ignition airflow rates can be obtained by solving Eq. (4) if high-temperature zone structure has no change after ignition, as shown in Eq. (5).

$$\Delta P_{post} = \Delta P_1 + \Delta P_2 = \Delta P_{pre} \quad \text{..... (4)}$$

$$u_{post} = \frac{(4CD + B^2)^{1/2} - B}{2D} \quad \text{..... (5)}$$

$$B = \frac{150(1-\varepsilon)}{d}\left(\mu_1 l_1 + \mu_2 l_2 \frac{T_2}{T_1} \right) \quad \text{..... (6)}$$

$$C = \left(150\frac{(1-\varepsilon)\mu}{d}u_{pre} + 1.75\rho{u_{pre}}^2 \right) H \quad \text{..... (7)}$$

$$D = 1.75\rho_1 l_1 + 1.75\rho_1 \frac{T_2}{T_1} l_2 \quad \text{..... (8)}$$

Where, u_{pre} is pre-ignition airflow rate, m/s, u_{post} is post-ignition airflow rate when high-temperature zone structure

has no change, m/s. B, C, D are some middle terms during calculation for simplifying Eq. (5).

When quartz sand blend was used maximum bed temperature was about 850°C. Quartz bed temperature in high temperature zone is not as high as sinter bed temperature (above 1 300°C) due to mismatching of flame front and heat front. When quartz sand blend was used, we can find the region above 400°C is about 100−250 mm, which also controls the sinter bed flow resistance. Bed zone above 400°C is defined as high temperature zone. **Figure 4** shows that measured airflow rate is 165 m^3/h in the upper layer and 105 m^3/h in the middle layer for case 1, 160 m^3/h in the upper layer and 120 m^3/h in the middle layer for case 2 when iron ores are replaced by quart sand and high-temperature zone structure has no change. According to measured temperature data, calculated post-ignition airflow rate is 193 m^3/h in the upper layer and 140 m^3/h in the middle layer for case 1 test, 190 m^3/h in the upper layer and 109 m^3/h in the middle layer for case 2. The calculation error is 16.97% for the upper layer and 33.33% for the middle layer in case 1, 18.75% for the upper layer and 9.17% for the middle layer in case 2. Though the error is a little big, due to difficulties in measuring bed temperature precisely, it is acceptable that Eq. (5) can predict post ignition airflow rate when bed structure has no change reasonably.

When iron ores and fluxes were replaced by quartz sand, there is no melt formation in the high-temperature zone and high-temperature zone structure is almost unchanged. Sinter pot tests in Fig. 4 have three layers structure and coke level in the middle layer is higher compared to those in other layers. Size distribution of coke used in different cases is showed in **Table 3**. Figure 4 shows airflow rate decreases sharply when high-temperature zone moves to mid-layer, from around 165 m^3/h to 105 m^3/h or around 160 m^3/h to 120 m^3/h; then airflow rate gradually increases when high-temperature zone moves to bottom layer. Sinter pot tests in **Fig. 5** are uniform bed. Figure 5 shows airflow rate gradually decreases with flame front descending down the bed until flame front reaches the bottom of sinter bed, from around 160 m^3/h to 110 m^3/h or around 150 m^3/h to 85 m^3/h. This proves that temperature has great influence on high-temperature zone resistance.

3.2. Impact of High-temperature Zone Structure on High-temperature Zone Flow Resistance

According to Eq. (5), the influence of temperature on airflow rate of sinter bed assuming high-temperature zone structure has no change was caculated, results are showed in **Table 4**. In sintering process, bed temperature and thickness of high temperature zone increases with high-temperature zone descending down the bed. As showed in Table 4, take the suction of 16 kPa as an example, calculated post-ignition airflow rate decreased from 129 m^3/h in upper layer to 93 m^3/h in bottom layer considering the effect of temperature only. However, measured airflow rate was relatively constant as 114 m^3/h until high-temperature zone gets to the bottom of the bed, which agrees well with previous work by Loo.[3] It is easy to find that if high-temperature zone structure has no change, post-ignition airflow rate will decreases gradually with high-temperature zone descending down the bed. **Figures 6** and **7** show the airflow rates with sinter blend at a suction of 8 kPa and 16 kPa; and there is no great change in airflow rate when high-temperature zone moves

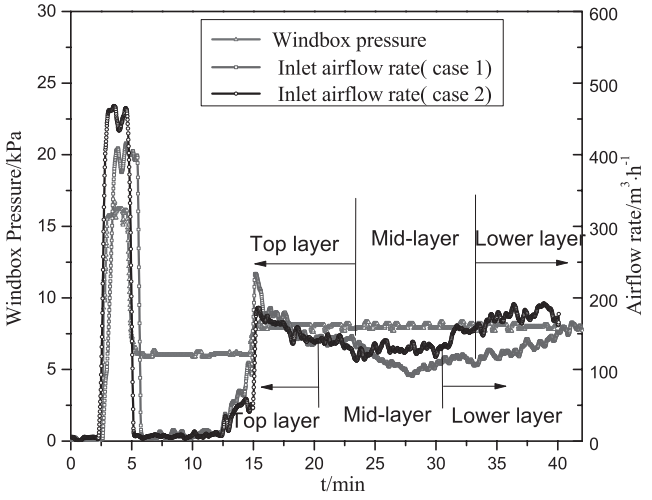

Fig. 4. Airflow rate curve of three-layer bed with only quartz sand and coke. Case 1: Coke size is full size distribution. Three-layer bed, 4.05 wt.%-4.85 wt.%-4.05 wt.% coke rate. Case 2: Coke size is −3.2 mm. Three-layer bed, 4.05 wt.%-4.85 wt.%-4.05 wt.% coke rate.

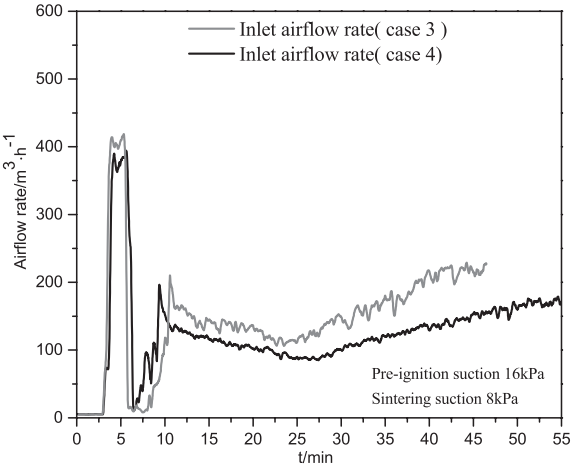

Fig. 5. Airflow rate curve of uniform bed with only quartz sand and coke. Case 3: Coke size is +1–2 mm. Uniform bed, 6.0 wt.% coke rate. Case 4: Coke size is −3.2 mm. Uniform bed, 6.0 wt.% coke rate.

Table 3. Cumulative mass passing of coke/%.

Item	Sieve size/mm									
	0.063	0.075	0.106	0.15	0.30	0.60	1.18	3.20	6.30	8.00
Full size	2.90	3.80	5.30	7.70	15.20	26.80	41.60	73.00	98.20	100.00
−3.2 mm	3.97	5.21	7.26	10.55	20.82	36.71	56.99	100.00	100.00	100.00

Table 4. Calculation and measured post-ignition airflow rates during iron ore sintering.

Test		Post-ignition airflow rate/$m^3 \cdot h^{-1}$			Pre-ignition airflow rate/$m^3 \cdot h^{-1}$	Suction/kPa
		Upper layer	Middle layer	Bottom layer		
1	Calculated*	129	101	93	198	16
	Measured		114			
2	Calculated	107	98	77	169	10
	Measured		102			
3	Calculated	72	55	41	118	6
	Measured		80			

* Calculated post-ignition airflow rate is the airflow rate when high-temperature zone structure has no change. Measured post-ignition airflow rate is the actual airflow rate during iron ore sintering.

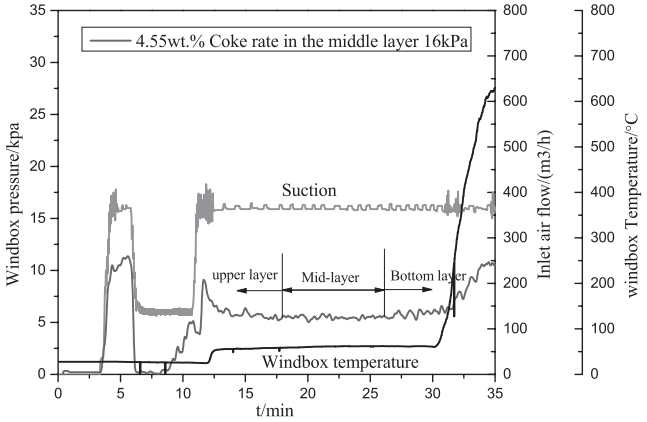

Fig. 6. Airflow rate curve of the 4.05 wt.%-4.55 wt.%-4.05 wt.% coke rate three-layer sinter bed.

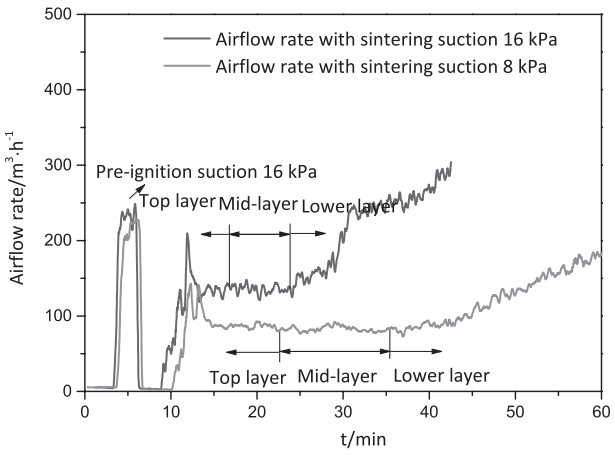

Fig. 7. Airflow rate curves of the 4.05 wt.%-4.85 wt.%-4.05 wt.% coke rate three-layer sinter bed.

to mid-layer with higher coke rate. This proves that high-temperature zone structure has changed to improve high-temperature zone permeability when sinter blend is used. Table 4 also shows that calculated post-ignition airflow rate is similar to measured post-ignition airflow rate or higher slightly than measured post-ignition airflow rate in the top layer, but is much lower than that measured post-ignition airflow rate in the bottom layer. This shows that the extent of high-temperature zone structure change in bottom layer is greater than that in top layer. The probable reason is that different melt volumes and viscosities result in the different high-temperature zone structures along the sinter bed height.

4. Factors Controlling Bed Temperature and High-temperature Zone Structure

4.1. Factors Controlling Bed Temperature during Iron Ore Sintering

During iron ore sintering, factors which affect bed temperature have been investigated widely. Altering coke rate can affect sinter bed temperature apparently. Decreasing basicity can lower energy consumption in the flame front, and result in higher sinter bed temperature. Suction has a great influence on bed temperature during iron ore sintering. Umadevi *et al.*[18] found that sinter bed temperature was higher when low suction was used. Increasing suction can increase airflow rate, which can take more energy away from the flame front. Altering coke particles size can also change sinter bed temperature, which can affect coke combustion efficiency. Loo[19] found that bed temperature with plus 2 mm coke particles was higher than that with full size. Increasing blend moisture will lower bed temperature. Loo[20] pointed out that increasing the content of goethitic ore in blend increased the moisture content, but the effect on addition required energy to dehydrate goethites is small.

4.2. Factors Controlling High-temperature Zone Structure during Iron Ore Sintering

4.2.1. Influence of Driving Force and Melt Volume on High-temperature Zone Structure

Figures 6, 7 and **8** show that when coke rate is altered, high-temperature zone resistance is relatively constant and has no great change at high suction. In other cases, gas flow rate drops sharply, particularly when low suction is used. When coke rate was increased, sinter bed temperature would increase.[2] This will results in gas expansion in the high-temperature zone, which can increase high-temperature zone resistance. High temperature can increase melt formation.[2,17,21,22] This will increase the change of high-temperature zone structure and improve high-temperature zone permeability. **Table 5** shows more details about airflow rate variation in the high-temperature zone. The decrease of airflow rate in high-temperature zone is less than gas expansion in high-temperature zone except for that in the bottom layer at a suction of 8 kPa when coke rate was increased. Airflow rate decreases greatly in the bottom layer with high coke rate at a suction of 8 kPa. This shows that airflow volume in the high-temperature zone relatively increases except for that in the bottom layer with high coke rate at low suction.

This suggests that gas channels in the high-temperature zone are dilated, and there are more gas channels or wider gas channels in the high-temperature zone.

Figure 8 shows that airflow rate in the bottom layer decreases sharply at low suction, but has no great change at high suction. Temperature in the bottom layer is very high because air for combustion is pre-heated. When coke rate in the bottom layer was increased to 4.85 wt.%, sinter bed temperature increases further. There are more melts in the high-temperature zone. This benefits gas channels formation in high-temperature zone and reduce high-temperature zone resistance. But excess melt in high-temperature zone would have a detrimental effect on high-temperature zone permeability.[7,8] Figure 8 and Table 5 also indicate that gas momentum has relatively strong influence on diluting or dilating gas channels.

4.2.2. Influence of Melt Viscosity on High-temperature Zone Structure

Figure 9 shows that there is the change in airflow rate in the bottom layer with different basicity. Airflow rate in the bottom layer decreases by 18.7% with low basicity and increases apparently with high basicity. Table 5 shows that gas expansions is less than the reduction of airflow rate in the high-temperature zone. Altering basicity can change melting point and melt fluidity. Decreasing basicity can raise melting point and viscosity,[17,21,22] which results in less melt and high viscosity. This indicates that melt has a very important role on gas channels formation and inadequate melt volume and high viscosity melt can increase high-temperature zone flow resistance. So melt with proper properties is very important for gas channels in high-temperature zone, melt acts as lubricant in high-temperature zone.[17]

As mentioned in the introduction, Loo[4] proposed that when pisolite ore was introduced during iron ore sintering high-temperature zone resistance would not deteriorate although pisolite ore had good assimilation which could benefit melt formation. This shows that there is no excess melt formation during pisolite ore sintering and good pisolite ore assimilation has no negative impact on sinter bed resistance. Respectively, good assimilation can improve sinter quality.

4.2.3. Influence of Green Bed Permeability on High-temperature Zone Structure

Table 6 shows the changes of airflow rate in different layers when green bed permeability is improved. Table 6 indicates that airflow rate increases in the middle layer and decreases in the top layer when coarser coke is used. During iron ore sintering suction is maintained to a certain value, the increase or decrease of airflow rate suggests bed flow resistance decreases or increases. Combing the discussions in section 4.2.1 and 4.2.2, they show that high-temperature zone flow resistance depends on drive force, bed voidage, melt volume and fluidity. Increasing coke particles can increase granule mean size and bed voidage,[9] this would increase gas channels in the high-temperature zone and reduce high-temperature zone flow resistance. Coke combustion starts in the leading edge and ends in the trailing

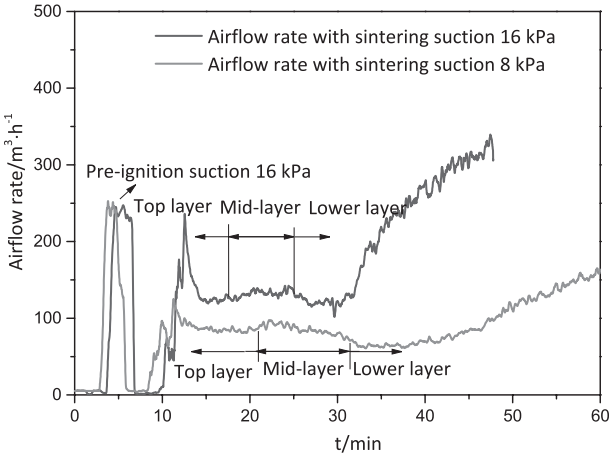

Fig. 8. Airflow rate curves of the 4.85 wt.%-4.05 wt.%-4.85 wt.% coke rate three-layer sinter bed.

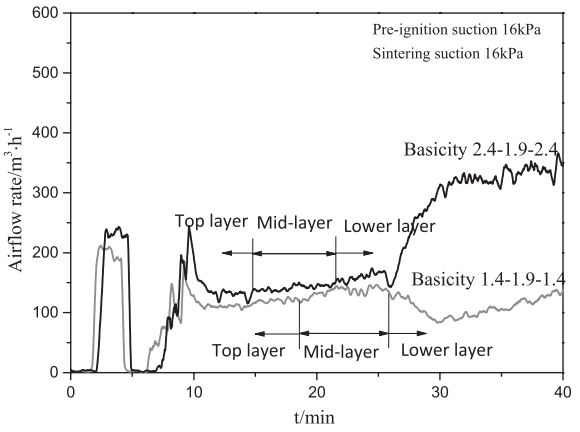

Fig. 9. Airflow rate curves with different basicity in the top and bottom layers.

Table 5. Comparison between variation of airflow rate and gas expansion in high-temperature zone compared with base condition.

Layer	Variation of airflow rate in high-temperature zone*	Gas expansion in the high-temperature zone	Variation of airflow rate in high-temperature zone	Gas expansion in the high-temperature zone
	Coke rate 4.85 wt.% 8 kPa		Coke rate 4.85 wt.% 16 kPa	
Upper layer	−0.4%	6.4%	−7.1%	6.2%
Central layer	−4.3%	7.5%	1.0%	5.6%
Lower layer	−25.3%	7.8%	−9.1%	10.7%
	Basicity 1.4		−	
Lower layer	−18.7%	2.9%	−	−

*Variation of airflow rate was calculated on the basis of the top layer average airflow rate because airflow rate remains relatively constant until close to burn-through.[3]

Table 6. Airflow rate and green bed permeability in different layers.

Item		Airflow rate/$m^3 \cdot h^{-1}$		Green bed permeability/JPU*	
variable		Upper layer	Middle layer	Upper layer	Middle layer
Coke size	Full size −+1.0 mm− Full size	129	147	19.6	23.3
Coke size	+1.0 mm−Full size−+1.0 mm	115	135		
Coke size	Full size −+0.5 mm− Full size	125	137.4	20.4	22.3
Coke size	+0.5 mm−Full size−+0.5 mm	118	128	22.3	20.4
Moisture		Average airflow rate/$m^3 \cdot h^{-1}$		−	
6.6 wt.%		138		24.1	
6.3 wt.%		120		17.8	

*JPU was calculated according to pre-ignition airflow rate under 16 kPa.

edge in the flame front.[23] Flame front width will be narrowed with removing fine coke particles when sinter bed temperature is relatively high;[1–3,9] this means that high-temperature zone is narrower. While, at low temperature large coke particles still combust in the trailing edge, flame front width will be extended.[23,24] Increasing green bed permeability by adding moisture can have a larger bed voidage, which favor more gas channels in high-temperature zone. But there is little advantage after exceeding a certain sinter airflow rate value. Because granules with thick adhering fines layer break down in dried zone tempestuously and has no much improvement in gas channels. And if green bed permeability is improved by adding too much moisture, humidified bed resistance increases. Both can increase sinter bed resistance and decrease airflow rate.

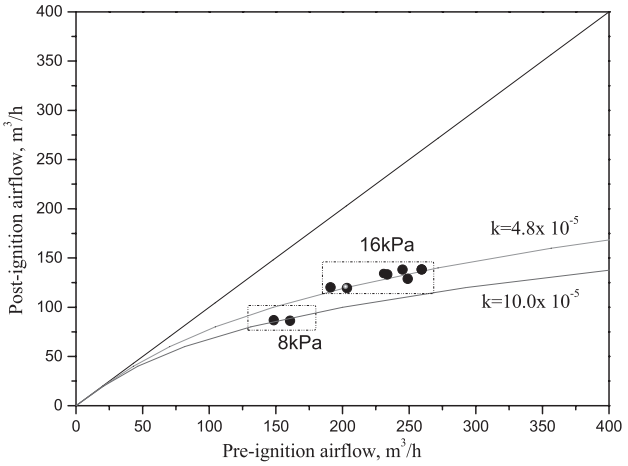

Fig. 10. Relationship between green bed airflow rate and sintering airflow rate under base condition.

5. Proposing k_5 Model

After ignition high-temperature zone is established and descends down the bed at the action of suction, which determines sinter bed flow resistance.[3–5] Due to high temperature and melt in the high-temperature zone, an additional resistance is introduced into sinter bed and sintering airflow rate decreases dramatically. Loo[4] found the relationship between pre-ignition and post-ignition airflow rate, which could be expressed by:

$$V_s = V_{pre} - k_5 V_s^3 \quad \text{..... (9)}$$

where V_s is post-ignition airflow rate, V_{pre} is pre-ignition airflow rate, k_5 is a constant which depends on sinter mix composition. k_5 shows the magnitude of high-temperature zone flow resistance. When k_5 is equal to zero, it indicates that high-temperature zone flow resistance is same as green bed and has no effect on sinter bed flow resistance. When k_5 is not equal to zero and greater than zero, Eq. (9) indicated that post-ignition airflow rate would decrease with a higher k value and high-temperature zone resistance is much greater.

Figure 10 shows the relationship between pre-ignition and post-ignition airflow rate for base blend, where different per-ignition airflow rate can be obtained by varying moisture.[4] The best fit curve for experimental data is the line with a k value of 4.8×10^{-5} at 16 kPa. In Fig. 4 data points at the suction of 8 kPa are below the best curve and its best fit curve is a line with a k value of 10×10^{-5}. This indicates that there is greater high-temperature zone resistance at low suction, which agrees with Loo's results.[4,5]

High-temperature zone resistance depends on high-temperature zone temperature and high-temperature zone structure. As discussed above high-temperature zone structure is relative to drive force, melt properties, bed voidage and high temperature zone thickness. Driving force can dilute or dilate gas channels and better fluidity favors gas channels formation. In the high-temperature zone proper melt is very important for high-temperature zone structure, but excess melt in high-temperature zone is adverse to high-temperature zone permeability and greater drive force is needed to move melts to form gas channels. So k_5 can also be expressed the Eq. (10).

$$k_5 = f(temperature) * f(structure) = \frac{V_{pre} - V_{post}}{(V_{post})^3} * f(\beta, \mu, \gamma, \xi_0, h) \quad \text{..... (10)}$$

Where β is melt fraction, μ is melt viscosity, γ is average drive force (the initial unit pressure drop of sinter bed), ξ_0 is initial voidage, h is high temperature zone thickness, V_{pre} is pre-ignition airflow rate, m^3/h, V_{post} is post-ignition airflow rate, m^3/h, V_{post} can be obtained according to Eq. (8). Melt fraction could be determined by Ref. 2), it can be expressed by the Eq. (11).

$$\beta=\begin{cases}1 & , \quad T_s > T_E \\ \left(\dfrac{T_s-T_M}{T_E-T_M}\right)^{\gamma} & , T_M \le T_S \le T_E \\ 0 & , \quad T_s < T_M\end{cases} \quad \text{..... (11)}$$

Where T_s is solid temperature; T_M is melting point temperature; T_E is the temperature that all the solids are melted. γ is the phase change factor.

During iron ore sintering adhering fine layer starts to melt, and then nuclei particles are assimilated gradually. Melt will encapsulate the nuclei particles until nuclei particles melt completely. When airflow goes through the high-temperature zone, airflow will contact with melt and airflow momentum will move melts and change the gas channels in the high-temperature zone. So melt viscosity outside the nuclei particles will have great effect on gas channel. Viscosity (μ) of the melt outside the nuclei particles could be determined by the Eq. (12).[19,20]

$$\mu = A\mu_0 EXP\left(\frac{E}{Bi^*}\right) \quad \text{..... (12)}$$

$$\mathrm{A} = 1.745 - 1.962*10^{-3}\mathrm{T} + 7.000*10^{-7}\mathrm{T}^2 \quad \text{..... (13)}$$

$$\mathrm{E} = 11.11 - 3.65*10^{-3}\mathrm{T} \quad \text{..... (14)}$$

$$Bi^* = \frac{\partial_{CaO}W_{CaO} + \partial_{MgO}W_{MgO} + \partial_{FeO}W_{FeO}}{\partial_{Fe_2O_3(aci.)}W_{Fe_2O_3} + \partial_{SiO_2}W_{SiO_2} + \partial_{Al_2O_3}W_{Al_2O_3}} \quad \text{... (15)}$$

$$\mu_0 = \sum \mu_{0i}X_i \quad \text{..... (16)}$$

In Eq. (16), Bi^* is a modified basicity index obtained from the composition of raw materials and the intrinsic coefficient ∂_i. X_i is mole concentration. μ_0 is the viscosity when the melt is a monomolecular system. W_i is the weight ratio of each component.[25,26] μ_0 and ∂_i are shown in the Refs. 25) and 26).

In order to calculate k_5 it is necessary to obtain the relationship between f (*structure*) and melt fraction, melt viscosity, drive force, initial voidage and high temperature zone thickness. Support vector machine (SVM) is a learning model on the basis of statistic learning theory and the principle of structure risk minimization and has good learning ability and generalization performance.[27–32] SVM is widely used in data regression, classification and forecasting.[27,29] SVM is more suitable for processing small samples with multidimensional and nonlinear data than other models, such as artificial neural network.[27,28] In this work SVM model was used to establish the relationship between f (*structure*) and melt fraction, melt viscosity, drive force, initial voidage and high temperature zone thickness.

The principle of SVM for regression is to construct a hyper plane; data can be regressed linearly by using the hyper plane in multi-dimensional or low-dimensional space.[27] When non-linear input data in low dimensional space is mapped into high dimensional feature space, it can be converted into linear data and be regressed in the feature space.[28] The regression function can be expressed as follows,[29]

$$f(x) = w\phi(x) + b \quad \text{..... (17)}$$

Where b is the bias, w is weight vector, $\phi(x)$ is the high dimensional feature space. w and b can be estimated by solving the following problem,[28,29]

$$\min_{w,b,\xi} \frac{1}{2}\| w \|^2 + C\sum_{i=1}^{n}\left(\zeta_i + \zeta_i^*\right) \quad \text{..... (18)}$$

$$\text{Subjected to } | y_i - < w\phi(x) > - b | < \varepsilon + \zeta_i ,$$

$$\zeta_i^* \ge 0, \zeta_i \ge 0, i = 1,2,\ldots,n$$

Where C is the penalty parameter, ζ_i^* and ζ_i are the positive slack variables. For solving the optimization problem, the decision function can be expressed as follows,[28,29]

$$f(x, a_i, a_i^*) = \sum_{i=1}^{n}(a_i - a_i^*)k(x_i, x) + b \quad \text{..... (19)}$$

Where $k(x_i, x)$ is kernel function, the value of kernel function is the inner product of two vectors in high dimensional feature space. In present work, the Radial Basis Function (RBF) is used as kernel function.[27]

$$k(x_i, x) = \exp(-\gamma \| x_i - x \|^2) \quad \text{..... (20)}$$

Where γ is the kernel parameter. The procedures processing the data by SVM include five steps, namely data scaling, the selection for kernel function, training, cross validation and test.[29] In this work training data and testing data are both scaled to the range [0, 1]. The Radial Basis Function (RBF) was selected as kernel function to analyze data. The kernel parameter (γ) and the penalty parameter (C) are very important parameters for SVM, in this work grid search was implemented to obtain them and cross validation was used to optimize the two parameters.

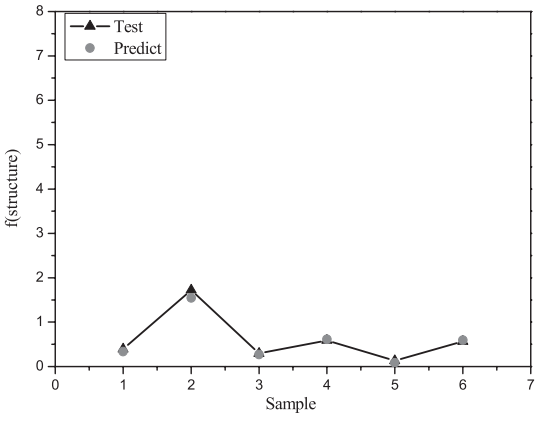

Fig. 11. Comparison between measured and predicted f (structure).

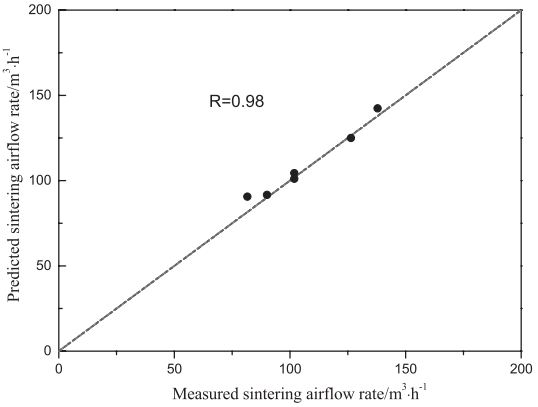

Fig. 12. Comparison between measured and predicted airflow rate.

In this work fifty-six sets of data from nineteen sinter pot tests in Zhao's PhD thesis[2] were used to validate our high-temperature zone resistance model. Data was divided into two groups randomly. 50 sets of data were used to train and 6 sets of data were used to test.

The squared correlation coefficient of fifty training data was 0.966 and the predicted f (*structure*) values of six testing data are shown in **Fig. 11**. The result suggests that SVM model can predict f (*structure*) well after training. Then k_5 can be calculated by Eq. (10) and predicted post-ignition airflow rates are obtained. **Figure 12** shows that post-ignition airflow rate can be predicted according to Eq. (10).

6. Conclusions

(1) Sinter bed temperature and high-temperature zone structure are the main factors determining the high-temperature zone resistence. Driving force can move melts and dilute or dilate gas channels to maintain sinter bed permeability. At high suction melt has relatively less impact on sinter bed permeability due to strong driving force.

(2) Melt has a very important impact on high-temperature zone resistance. Proper melt fraction can act as lubricant in high-temperature zone. It can favor driving force to form gas channels and reduce high-temperature zone resistance. But too much melt will increase the resistance of airflow flowing through high-temperature zone and need larger driving force to form gas channels. When coke rate was increased from 4.05 wt.% to 4.85 wt.% at a suction of 8 kPa, airflow rate in the bottom layer decreases by 25%.

(3) Increasing green bed permeability can increase the size of gas channels in the high-temperature zone. Changing green bed permeability can alter high-temperature zone resistance. It depends on the changes of melt formation and high-temperature zone thickness. Increasing coke size and limestone in the upper layer raises high-temperature zone resistance.

(4) When coke level is increased, high-temperature zone temperature increased but high-temperature zone resistance doesn't have great change at high suction because the gas airflow can dilate gas flow channels to maintain bed permeability. Gas flow rate drops sharply when low suction is used due to weak driving force.

(5) High-temperature zone structure is closely relative to driving force, melt properties and bed viodage. SVM model after training can simulate the impact of high-temperature zone structure on high-temperature zone resistance. High-temperature zone resistance model in this work is established and it can predict the sintering airflow rate associated with pre-ignition airflow rate.

Acknowledgment

This work was supported by National Natural Science Foundation of China (51476137), and National Basic Research Program of China (2015CB251501).

REFERENCES

1) C. S. Teo, R. A. Mikka and C. E. Loo: *ISIJ Int.*, **32** (1992), 1047.
2) J. P. Zhao: PhD Thesis, Zhejiang University, Hangzhou, (2012).
3) C. E. Loo and J. C. M. Leaney: *Trans. Inst. Min. Metall. Sect. C:Miner. Process. Extr. Metall.*, **111** (2002), 11.
4) C. E. Loo and M. F. Hutchens: *ISIJ Int.*, **43** (2003), 630.
5) C. E. Loo, N. Tame and G. C. Penny: *ISIJ Int.*, **52** (2012), 967.
6) J. S. Li and C. X. Chen: Dynamic of Fluids in Porous Media, ed. by J. Bear, China Architecture & Building Press, Beijing, (1983).
7) N. Oyama, H. Sato, K. Takeda, , T. Ariyama, S. Masumoto, T. Jinno and N. Fujii: *ISIJ Int.*, **45** (2005), 817.
8) E. Kasai, S. Komarov, K. Nushiro and M, Nakano: *ISIJ Int.*, **45** (2005), 538.
9) D. O'D, Q. Sun, H. B. Shen, L. J. Yan and H. Z. Shi: *Iron Steel*, **43** (2008), 8.
10) H. Zhou, Z. H. Liu, M. Cheng and R. P. Liu: *Energ. Fuel.*, **29** (2015), 974.
11) Z. Y. Zou, T. Z. Huang, X. S. Yang and J. Chen: *Trans. NF Soc.*, **5** (1995), 15.
12) N. K. Nath and K. Mitra: *Mater. Manuf. Process.*, **20** (2005), 335.
13) M. J. Cumming, W. J. Rankin, J. R. Siemon, J. A. Thurlby, G. J. Thornton, E. A. Kowalczyk and R. J. Batterham: Proc. 4th Int. Symp. on Agglomeration, ISS, Warrendale, PA, (1985), 763.
14) M. J. Cumming and J. A. Thurlby: *Ironmaking Steelmaking*, **17** (1990), 245.
15) R. Venkataramana, S.S. Gupta and P.C. Kapur: *Int. J. Miner. Process.*, **57** (1999), 43.
16) H. M. Long: PhD Thesis, Central South University, Changsha, (2007).
17) J. Y. Fu, T. Jiang and D. Q. Zhu: Sintering and Pelletizing, Central South University of Technology Press, Changsha, China, (1996).
18) T. Umadevi, A. Brahmacharyulu, R. Sah and P. C. Mahapatra: *Ironmaking Steelmaking*, **41** (2014), 410.
19) C. E. Loo: *Ironmaking Steelmaking*, **18** (1991), 33.
20) C. E. Loo: *ISIJ Int.*, **45** (2005), 436.
21) C. E. Loo and W. Leung: *ISIJ Int.*, **43** (2003), 1393.
22) D. Debrincat, C. E. Loo and M. F. Hutchens: *ISIJ Int.*, **44** (2004), 1308.
23) C. E. Loo: *Trans. Inst. Min. Metall. Sect. C: Miner. Process. Extr. Metall.*, **109** (2000), 11.
24) K. F. Cen, Q. Yao, Z. Y. Luo and X. Gao: Combustion Theory and Pollutants Control, Zhejiang University Press, Hangzhou, (2002).
25) S. Machida and K. Nushiro: *ISIJ Int.*, **45** (2005), 513.
26) T. Iina, H. Saka, Y. Klta and K. Shigeno: *ISIJ Int.*, **40** (2000), S110.
27) H. Zhou, Q. Tang, L. B. Yang, Y. Yan, G. Lu and K. F. Cen: *Fuel*, **117** (2014), 944.
28) J. M. Hu, J. Z. Wang and G. W. Zeng: *Renew. Energ.*, **60** (2013), 185.
29) J. L. Chen, G. S. Li and S. J. Wu: *Energ. Convers. Manage.*, **75** (2013), 311.
30) C. Cortes and V. Vapnik: *Machine Learning*, **20** (1995), No. 3, 273.
31) C. Chang and C. Lin: *ACM Trans. Intelligent Syst. Technol.*, **2** (2011), 27.
32) B. T. Zhao, Z. X. Zhang and X. J. Wu: *Energ. Fuel.*, **24** (2010), 3066.